Transactions of the Materials Research Society of Japan 25 [4] 1065-1068 (2000)

Production and Mechanical Properties of Al-M (M : Cr, V, Ti) Base Alloys containing Aperiodic Nano-Particles

H. M. Kimura, A. Inoue and K. Sasamori
Institute for Materials Reserch, Tohoku University, Sendai 980-8577
Fax: 81-22-215-2159, e-mail: hisami@imr.tohoku.ac.jp

The fcc-Al plus quasicrystalline structure was formed in the range of 4 to 16 at%Cr. The Vickers hardness of the $Al_{84.6}Cr_{15.4}$ alloy with a mostly single quasicrystalline phase was 710. The addition of Ce and Co in the Al-Cr binary alloys was effective for the extension of the concentration range of the quasicrystalline phase to a lower solute concentration range. The fracture strength (σ_f) increased to 1340 MPa for the $Al_{94.5}Cr_3Ce_1Co_{1.5}$ alloy in which the particle size and volume fraction were about 40 nm and 70 %, respectively. The σ_f of the $Al_{94}V_4Fe_2$ alloy was 1390 MPa and the particle size and volume fraction were about 13 nm and 50 %, respectively. Similarly, σ_f of the $Al_{93}Ti_4Fe_3$ alloy was 1320 MPa and the particle size and volume fraction were about 12 nm and 30 %, respectively. In the aluminum alloys containing nanoscale quasicrystalline and amorphous particles, the 0.2 % proof stress ($\sigma_{0.2}$) increased with decreasing particle size up to about 25 nm. The further decrease in particle size to less than about 25 nm, $\sigma_{0.2}$ is almost constant. The Hall-Petch relation was recognized between $\sigma_{0.2}$ and $d_s^{-1/2}$ in the average diameter of particle (d_s) range over 25 nm.

Key words: mechanical property, aluminum base alloy, nanoscale particle, quasicrystalline phase, amorphous phase

1. INTRODUCTION

Inoue et al. have found that amorphous $Al_{88}(Y_{1-x}Ce_x)_2Ni_9Fe_1$ alloys containing nanoscale fcc-Al particles exhibit tensile fracture strength and hardness higher than those of amorphous single phase alloys with the same compositions, without detriment to good bending ductility[1]. In this paper, we have studied the microstructure, mechanical properties of rapidly solidified Al-Cr, Al-Cr-Ce-Co, Al-V-Fe and Al-Ti-M (M: transition metal) alloys containing nanoscale quasicrystalline and amorphous particles.

2. EXPERIMENTAL PROCEDURE

Melt-spun ribbons with about 15 μm thickness and 0.5 ~ 1.0 mm width were prepared by a single roller melt-spinning technique in an argon atmosphere. Microstructure of as-quenched alloys was examined by X-ray diffractometry and transmission electron microscopy (TEM). Tensile strength and hardness of the ribbon specimens were measured by an Instron-type tensile machine and Vickers microhardness tester, respectively.

3. RESULTS AND DISCUSSION

3.1 Rapidly solidified Al-Cr alloys

In order to clarify the change in microstructural features of the Al-Cr quasicrystals with chromium concentration, TEM observations were made for the rapidly solidfied $Al_{100-x}Cr_x$ (x = 4 to 18 at%) alloys. As

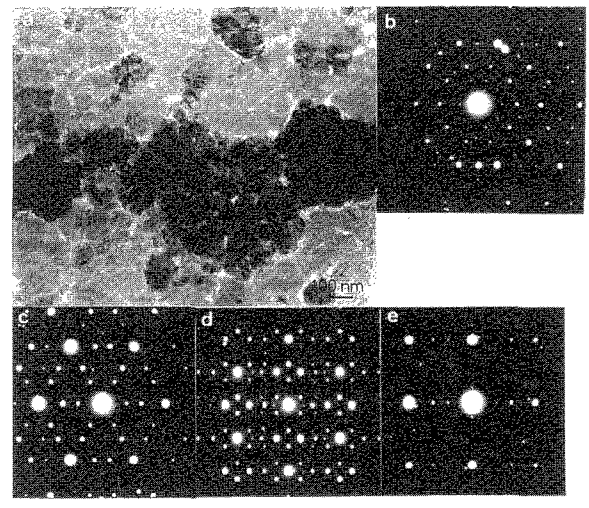

Figure 1 Bright-field electron micrograph (a) and selected-area electron diffraction patterns (b to e) of a rapidly solidified $Al_{95.5}Cr_{14.5}$ alloy

exemplified in Figure 1, The $Al_{85.5}Cr_{14.5}$ alloy appears to consist only of a quasicrystal. Their patterns reveal the five-, three- and two-fold symmetries of icosahedral quasicrystal. The fcc-Al plus quasicrystalline structure was formed in the range of 4 to 16 at%Cr. Figure 2 shows the change in Vickers hardness (Hv) as a function of chrominum concentration of rapidly solidified Al-Cr alloys, together with the data of rapidly solidified Al-Mn

alloys. Hv is about 255 for $Al_{90}Cr_{10}$, increases gradually with an increase in chrominum and rapidly at compositions 14.5 at % Cr and reaches 710 for $Al_{84.6}Cr_{15.4}$ alloy with an almost single quasicrystalline phase. The Hv of the Al-Cr quasicrystal is lower by 300 than that (≒1010) of $Al_{77.5}Mn_{22.5}$ alloy with an almost single quasicrystalline phase.

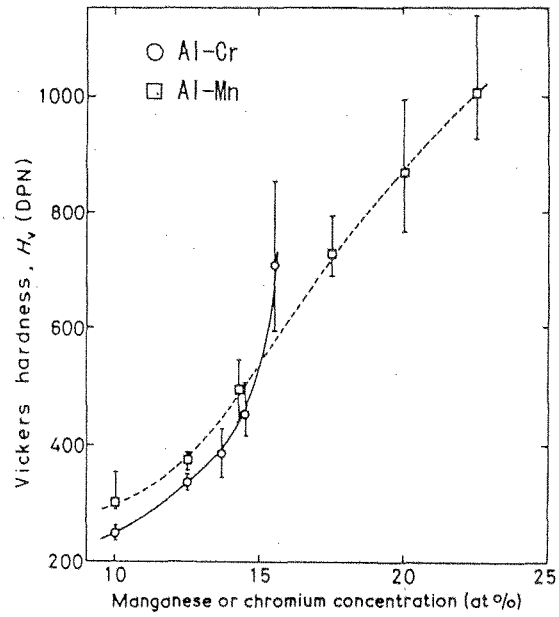

Figure 2 Vickers hardness (Hv) of rapidly solidified Al-Cr alloys as a function of chrominum content. The data of rapidly solidified Al-Mn alloys are also shown for comparison. Load : 25 g. □, Al-Mn ; ○, Al-Cr.

3.2 Rapidly solidified Al-Cr-Ce-Co alloys

The addition of Ce and Co in the Al-Cr binary alloys was effective for the extension of the concentration range of the quasicrystalline phase to a lower solute concentration range. Figure 3 shows a bright-field electron micrograph (a), selected-area electron diffraction pattern and its identified result (b) and dark-field electron micrograph (c) taken from a part of the (211111) and (221001) reflection rings for the rapidly solidified $Al_{94.5}Cr_3Ce_1Co_{1.5}$ alloy. It is seen that the icosahedral particles containing a high density of phason defects with a particle size of about 40 nm distribute in a surrounded state with a thin Al layer. These features are just the same as the previous data for rapidly solidified Al-Mn-Ce[2),(3)] and Al-Cr-Ce[3)] alloys consisting of nanoscale icosahedral particles surrounded by a thin Al phase. Figure 4 shows the compositional dependence of tensile fracture strength (σ_f) and bending ductility for rapidly solidified $Al_{99-x-y}Cr_xCe_1Co_y$ alloys. The ductile alloys which can be bent through 180 degrees are obtained in the solute concentration range less than 5 at%. The numbers in the figure represent σ_f values. The high σ_f values above 1000 MPa combined with good bending ductility are obtained in the range of 3 to 4%Cr and 1 to 2%Co and the highest σ_f is 1340 MPa for $Al_{94.5}Cr_3Ce_1Co_{1.5}$ alloy.

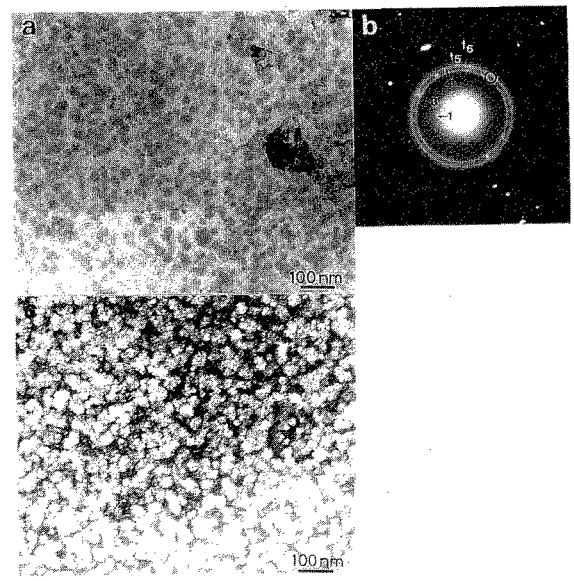

Figure 3 Bright-field electron micrograph (a), selected-area electron diffraction pattern (b) and dark-field electron micrograph (c) taken from a part of $(211111)_i$ and $(221001)_i$ reflection rings for a rapidly solidified $Al_{94.5}Cr_3Ce_1Co_{1.5}$ alloy. The reflection rings of 1, 3, 4, 5 and 6 are identified to be (111100), (211111), (221001), (322101) and (332002), respectively.

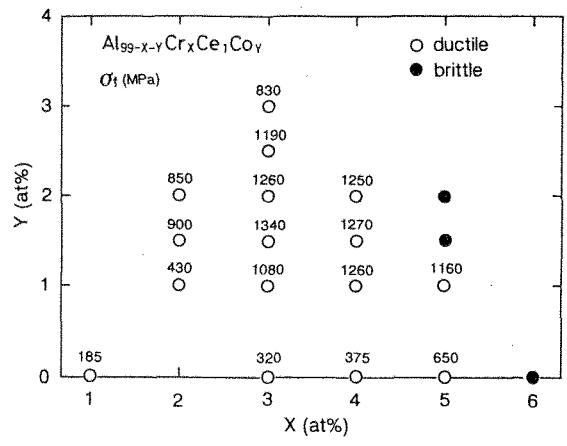

Figure 4 Compositional dependence of tensile fracture strength (σ_f) and bending ductility for rapidly solidified $Al_{99-X-Y}Cr_XCe_1Co_Y$ alloys.

3.3 Rapidly solidified $Al_{94}V_4Fe_2$ alloy

Figure 5 shows a bright-field electron micrograph (a), the selected-area electron diffraction pattern (b) and dark-field electron micrographs (c and d) taken from a

part of the broad halo ring for the rapidly solidified $Al_{94}V_4Fe_2$ alloy. The bright- and dark-field images indicate that the Al phase with the dark contrast and the amorphous phase with the bright contrast have the phase regions of about 7 nm and 10 nm, respectively, and are coexistent in a randomly mixed state. Figure 6 shows the changes with testing temperature in tensile fracture strength (σ_f), 0.2% proof stress ($\sigma_{0.2}$) and total fracture elongation including elastic elongation (ε_f) of the rapidly solidified $Al_{94}V_4Fe_2$ alloy. The tensile fracture strength of the Al-V-Fe alloy decreases gradually from 1390 to 620 MPa in the temperature range from room temperature to 680 K. On the other hand, the ε_f increases slightly from 2.6 to 4.3% at the temperatures below 640 K and then significantly to 3.9% with increasing temperature to 680 K. The high values of 900 MPa for σ_f, 640 MPa for $\sigma_{0.2}$ and 4.3% for ε_f are retained at 640 K and the further increase in testing temperature causes significant decreases in σ_f and $\sigma_{0.2}$ to 540 and 620 MPa, respetively, at 680 K and a rapid increase in ε_f to 22%.

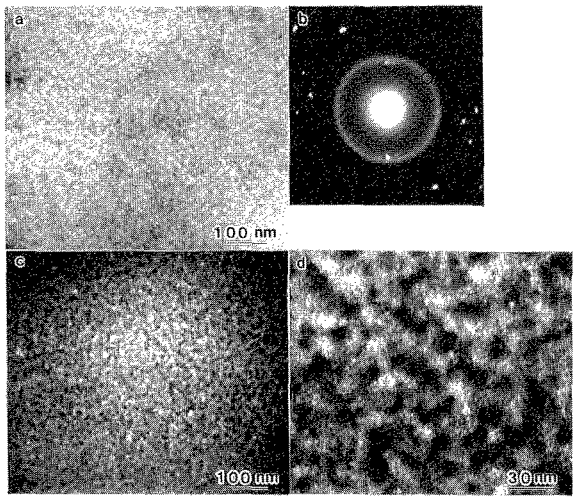

Figure 5 Bright-field electron micrograph (a), selected-area electron diffraction pattern (b) and dark-field electron micrographs (c and d) of a rapidly solidified $Al_{94}V_4Fe_2$ alloy. The dark-field electron micrographs (c) and (d) were taken from a part of the halo ring in (b).

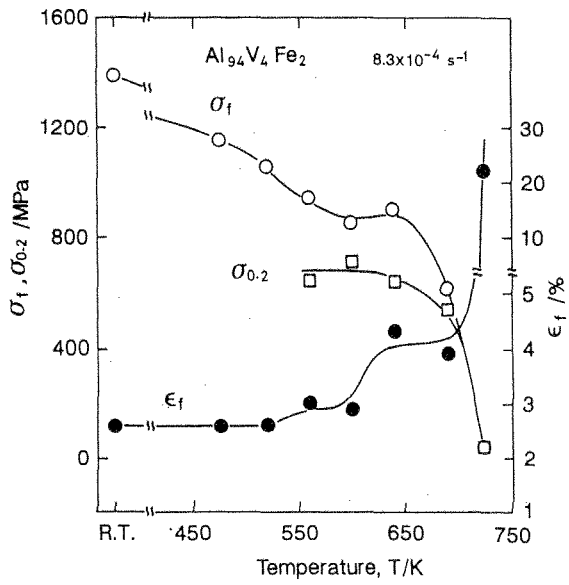

Figure 6 Changes in 0.2% proof stress ($\sigma_{0.2}$), tensile fracture strength (σ_f) and fracture elongation (ε_f) with testing temperature of a rapidly solidified $Al_{94}V_4Fe_2$ alloy.

3.4 Rapidly solidified Al-Ti-Fe alloy

Figure 7 shows a bright-field electron micrograph (a), selected-area electron diffraction pattern (b) and dark-field electron micrographs (c and d) taken from a part of the broad halo ring for the rapidly solidified $Al_{93}Ti_4Fe_3$ alloy. The electron diffraction pattern consists of halo ring and fcc-Al reflection spots. Furthermore, the granular amorphous phase with a size of about 11 nm is homogeneously coexistent with fcc-Al phase with a grain size of about 10 nm, indicating the formation of a nanogranular amorphous phase.

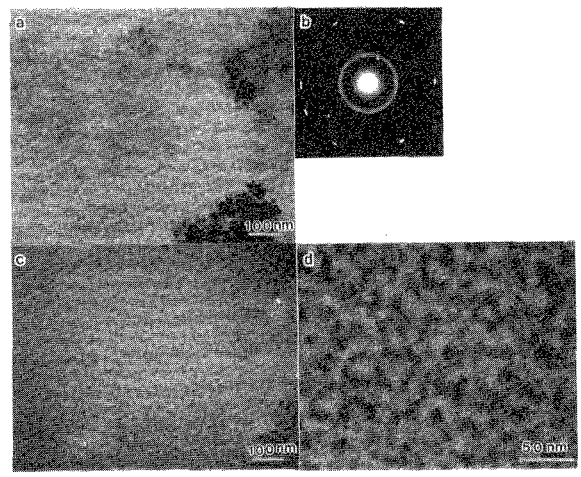

Figure 7 Bright-field electron micrograph (a), selected-area electron diffraction pattern (b) and dark-field electron micrographs (c and d) of a rapidly solidified $Al_{93}Ti_4Fe_3$ alloy. The dark-field electron micrographs (c) and (d) were taken from a part of the halo ring in (b).

Figure 8 shows tensile fracture strength (σ_f) and Vickers hardness (Hv) for the rapidly solidified $Al_{93}Ti_4M_3$ alloys. The V-, Fe-, Co- and Ni-containing alloys exhibit high tensile strength above 1000 MPa as well as high hardness above 360 and the largest σ_f and Hv values reach as high as 1320 MPa and 450 for the Fe-containing alloy. On the other hand, the Cr-, Mn- and Cu- containing alloys exhibit much lower σ_f and Hv

values. Thus, it is characterized that the higher mechanical strength is obtained for the nanogranular amorphous and fcc-Al phases, and the disappearance of the amorphous phase by the precipitation of intermetallic compounds causes significant decreases in σ_f and Hv. The good correspondence indicates that the nanogranular mixed structure is useful for the achievement of high mechanical strength.

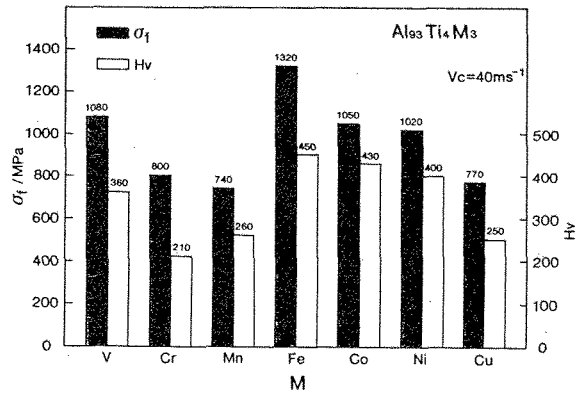

Figure 8 Tensile fracture strength (σ_f) and Vickers hardness (Hv) of rapidly solidified $Al_{93}Ti_4M_3$ (M:V, Cr, Mn, Fe, Co, Ni, Cu) alloys.

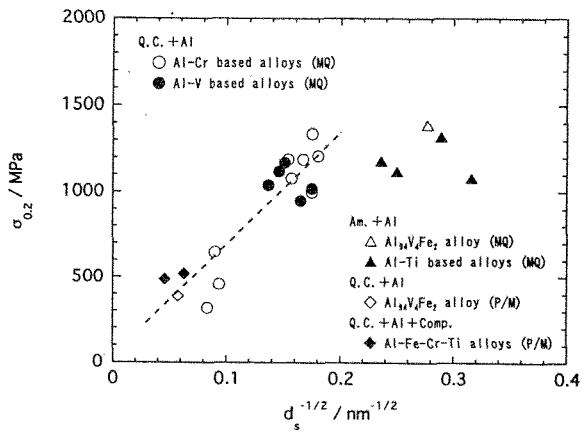

Figure 9 Hall-Petch relation between $\sigma_{0.2}$ and $d_s^{-1/2}$ for quasicrystalline base Al alloys in the melt-spun ribbon and extruded bulk forms. The d_s represents the spacing between the quasicrystalline and amorphous particles.

3.5 Strengthening mechanisms

It is important to discuss the strengthening mechanism for the Al-based alloys containing nanoscale nonperiodic phases in the as-spun ribbon and extruded bulk states of the Al-Cr-Ce-Co, Al-V-Fe, Al-Ti-Fe and Al-Fe-Cr-Ti systems. Figure 9 shows the Hall-Petch plot between the 0.2 % proof stress ($\sigma_{0.2}$) and $d_s^{-1/2}$ for the Al-based alloys. Here, d_s represents the distance between the surface of the quasicrystalline and amorphous particles. A good linear relation revealing the Hall-Petch relation is recognized in the d_s range over 25 nm and the further decrease in d_s leads to the deviation from the Hall-Petch relation. The fine structure with d_s below 25 nm has a unique strengthening mechanism which is different from that for the Hall-Petch relation. That is, the fine structure has a high volume fraction of interface boundary which cannot act as effective resistant barrier against movement of dislocations. The fine grain structure enables an easy sliding along interface boundary as well as a sinking of dislocations at the interface, leading to the absence of dislocations in the fcc-Al matrix.

4. CONCLUSIONS

The microstructure and mechanical properties of rapidly solidified Al-Cr, Al-Cr-Ce-Co, Al-V-Fe and Al-Ti-M (M: transition metal) alloys were examined, with the aim of developing ultra-high strength materials by utilizing the nanoscale mixed structure. The results obtained are summarized as follows.

(1) The fcc-Al plus quasicrystalline structure was formed in the range of 4 to 16 at%Cr. Vickers hardness is 710 for $Al_{84.6}Cr_{15.4}$ alloy with a quasicrystalline single phase.

(2) The coexistent nanoscale quasicrystalline and Al phases were obtained for the $Al_{94.5}Cr_3Ce_1Co_{1.5}$ alloy. The mixed phase alloy also has good bending ductility and the highest tensile fracture strength is 1340 MPa.

(3) The rapidly solidified $Al_{94}V_4Fe_2$ alloy with the coexistent amorphous and Al phases has good bending ductility and exhibits high tensile strength of 1390 MPa. The high tensile fracture strength above 1000 MPa is retained in the temperature range up to 650 K.

(4) A nanogranular amorphous and Al phases was formed in the rapidly solidified $Al_{93}Ti_4Fe_3$ alloy. The tensile fracture strength and Vickers hardness exhibit the highest values of 1320 MPa and 450, respectively.

(5) The Hall-Petch relation was recognized between $\sigma_{0.2}$ and $d_s^{-1/2}$ in the d_s range over 25 nm, but the further decrease of d_s led to the deviation from the Hall-Petch relation.

REFERENCES

(1) Y. H. Kim, A. Inoue and T. Masumoto, Keikinzoku (J. Jpn. Inst. Light Met.), **42, 217-223** (1991).

(2) A. Inoue, M. Watanabe, H. M. Kimura, F. Takahashi, A. Nagata and T. Masumoto, Mater. Trans., JIM, **33, 723-729** (1992).

(3) A. Inoue, M. Watanabe, H. M. Kimura and T. Masumoto, Sci. Rep. Res. Inst. Tohoku Univ., **38, 138-160** (1993).

(Received December 17, 1999; Accepted August 16, 2000)